

INDONESIAN JOURNAL ON GEOSCIENCE

Geological Agency Ministry of Energy and Mineral Resources

Journal homepage: https://ijog.geologi.esdm.go.id ISSN 2355-9314, e-ISSN 2355-9306



Spectral-Wise Method Derived by Optical Images For Phosphate Mineral Exploration In Mamuju, West Sulawesi, Indonesia

RAJAB KURNIAWAN^{1,2} and Asep Saepuloh¹

¹Geological Engineering Study Program, Faculty of Earth Sciences and Technology, Bandung Institute of Technology, Jl. Ganesha No.10, Bandung, West Java, Indonesia ²Department of Exploration and Mine Development, PT. Trimegah Bangun Persada Tbk., Jakarta, Indonesia

> Corresponding author: razens03@gmail.com Manuscript received: November, 08, 2024; revised: March, 29, 2025; approved: September, 24, 2025; available online: November, 20, 2025

Abstract - Phosphates are predominantly used in the manufacture of fertilizers for crop nutrition and the production of animal feed supplements. Only 10-15% of the world phosphate rock production has other uses, such as pharmaceuticals, ceramics, an important alternative source of rare earth elements (REE), and Lithium-Iron-Phosphate (LFP) batteries. In Indonesia, various types of rocks are composed of phosphate components, but rocks containing economic value are limited. They are generally found in sedimentary or biogenic phosphate deposits, whereas phosphate resources derived from igneous rocks are still undiscovered. Therefore, regionally accurate mapping using spectral-wise methods is proposed in this study. The five spectral references originated from phosphate minerals from the USGS spectral library were used: fluorapatite, chlorapatite, hydroxylapatite, monazite, and xenotime. The spectral-wise aims to identify anomalies of phosphate minerals based on the behaviour of spectral absorption at wavelength 2 μ m. Their spectra showed a similar absorption pattern at a wavelength of 2 μ m originating from orthophosphate (PO₄). This spectral-wise formulation was then applied to detect the phosphate occurrences using the Landsat 9 image. According to the proposed method, three PO₄ prospect zones could successfully be detected covering 2,604 Ha with P₂O₅ content reaching 1.14–2.73 %. It has been verified that the proposed method has an accuracy of about 70 % compared to rock samples containing P₂O₅ at the field study.

Keywords: Mamuju, phosphates, Landsat 9 image, spectral-wise method

© IJOG - 2025

How to cite this article:

Kurniawan, R. and Saepuloh, A., 2025. Spectral-Wise Method Derived by Optical Images For Phosphate Mineral Exploration In Mamuju, West Sulawesi, Indonesia. *Indonesian Journal on Geoscience*, 12 (3), p.467-480. DOI:10.17014/jjog.12.3.467-480

Introduction

Various rocks have phosphate-containing components such as phosphorite, francolite, and carbonatite (Ptacek, 2016). However, the rocks containing phosphate with economic value for mining materials are limited (Steiner *et al.*, 2015). Phosphate is commonly used as an industrial raw material. There are about 85 % raw phosphate material used for plant fertilizers and

animal supplements (Ptacek, 2016). The remaining usability is for industrial purposes such as pharmaceuticals, ceramics, textiles, and an alternative source for rare earth elements (Ptacek, 2016). The phosphate is also used for Lithium-Iron-Phosphate (LFP) electric vehicle batteries (Xu *et al.*, 2020). Phosphate deposits derived from igneous rocks, which are mostly found in carbonatite or other types of alkaline intrusions, are generally low grade, but high quality with

Indexed by: SCOPUS

low content of unwanted contaminants such as Cd, Pb, As, U (Ptacek, 2016).

In Indonesia, rock containing phosphate minerals is generally found in the sedimentary or biogenic phosphate deposits, whereas phosphate resources derived from igneous rocks are still undiscovered (Ptacek, 2016). Therefore, phosphate resources derived from igneous rocks become an interesting exploration target to be researched and sought after.

The Apatite $[Ca_s(PO_a)_3(OH, F, Cl)]$ is the most abundant phosphate mineral of all phosphorus in the earth crust (Ptacek, 2016). The apatite derived from intrusive igneous rocks, one of which is associated with alkaline rocks (Ptacek, 2016). The alkaline rocks are rich in alkali metals and feldspathoids (e.g. nepheline, leucite) (Abdullah et al., 2023). Primary apatite from igneous rock sources originated from chlorapatite, fluorapatite, or hydroxilapatite varieties (Ptacek, 2016). Monazite is a phosphate mineral containing light rare earth elements (LREE) found in a variety of rock types and also radioactive sources due to the presence of thorium and uranium (Ptacek, 2016). Xenotime is a rare earth phosphate mineral with the main component is yttrium orthophosphate (YPO₄) known as a heavy rare earth element (HREE). The association of phosphate elements with rare earth elements and radioactivity was reported by a previous study (Indrastomo et al., 2015; Ciputra et al., 2025).

Southwest Mamuju District, West Sulawesi Province, Indonesia, has been selected with a region of interest (ROI) of 30×30 km as the studied area (Figure 1). The studied area is composed of leucite-bearing lapilli tuffs, volcanic breccias, leucite basalt fragments, and leucite basalts of Adang Formation (Ratman and Atmawinata, 1993; in Shaban *et al.*, 2016). The leucite mineral was found in the phenocrysts of basalt rocks indicating feldspathoid lava with a high potassium content (Indrastomo *et al.*, 2015). The abundance of feldspathoid minerals is interpreted as an indication of phosphorus-bearing igneous rock. The purpose of this study is to determine the equation model for the presence of phosphate minerals based on spec-

tral absorption in the visible (VIS) - short wave infrared (SWIR) range, then to apply the equation model to detect the presence of phosphate minerals in the Mamuju area, and to analyze geological controls on the distribution of phosphate minerals.

Remote sensing using multispectral images with conventional methods commonly used for mineral identification is the band ratio equation. This method uses the comparison between peaks and absorb reflectance in the spectral signature of the target mineral with the approach of the wavelength values of the bands in the multispectral image (Landsat, ASTER, *etc.*). The drawback of this method is that for some spectral minerals the wavelength position of the multispectral image bands does not always represent the peak or absorb reflectance values of the spectral signature. So, the ratio equation results can not represent the specific target mineral and cause the resulting anomalous area distribution to be overestimated.

In this study, the application of the band ratio reveals that the target mineral, specifically the phosphate mineral apatite, which indicates the presence of phosphate, can not have its peak reflectance and absorption accurately represented by the wavelengths of the Landsat 9 image bands used. This is because the absorption pattern falls between these bands. Therefore, a specialized method is required to calculate the spectral absorption value of the phosphate mineral and convert it into the Landsat 9 image.

The spectral-wise method can be used to identify the phosphate element as a specific target mineral based on its spectral characteristics. In this case, the spectral characteristics of phosphate-bearing minerals are compared, so that it can be known that uniform absorption patterns will lead to the same element. This method can identify the absorption pattern between the wavelengths of the bands on Landsat 9. Then, the relationship between the reflectance value of the absorption and the two bands between them is illustrated to form an angle that can be calculated and converted into an angular index value that can be adjusted on the Landsat 9 image.

The workflow in this research is divided into three stages, starting from the data preparation

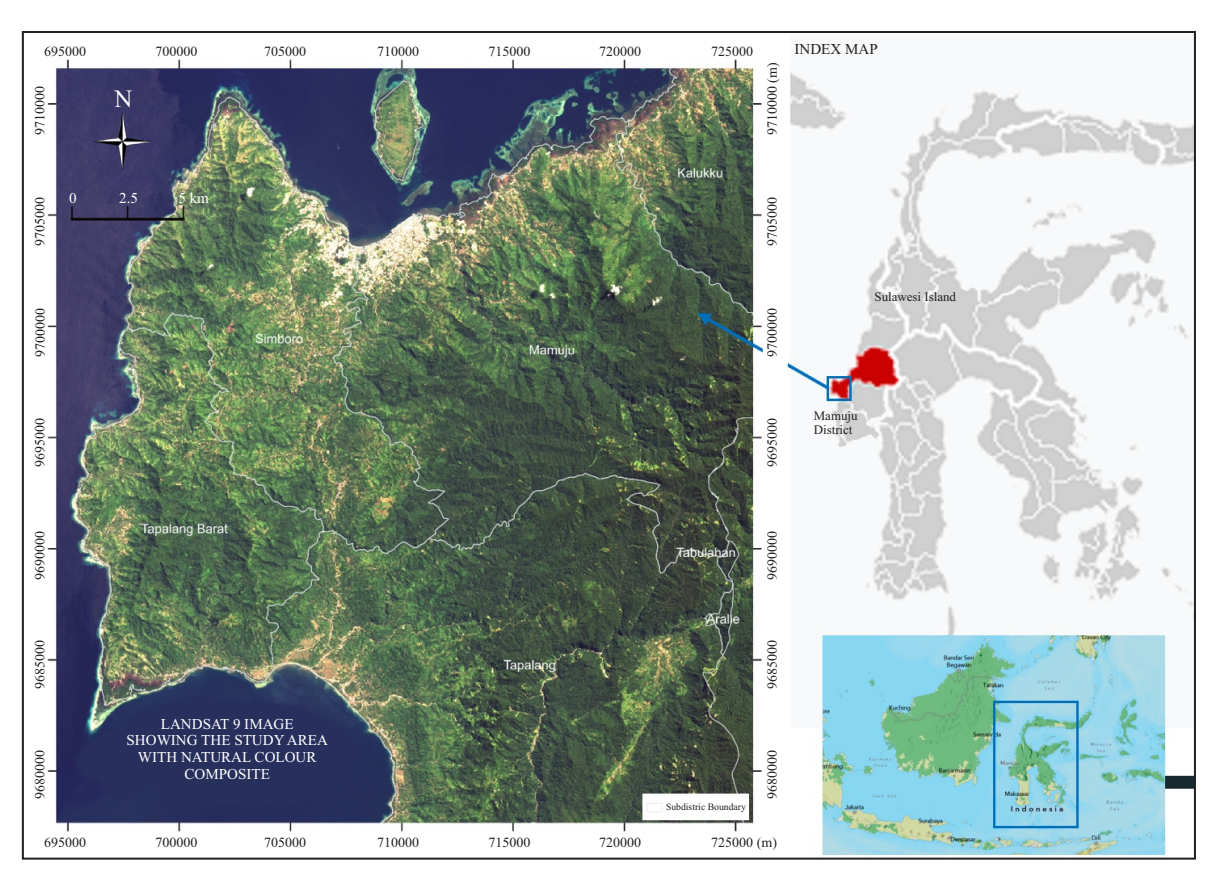


Figure 1 . The studied area is about 30×30 km in The Southwest Mamuju District, West Sulawesi Province, Indonesia, on the natural colour composite image of Landsat 9 (R, G, B=Band 4,3,2).

stage including literature studies, secondary data collection in the form of spectral signature (SS) of five phosphate minerals, Landsat 9 images, reference field sampling data results from previous studies, digital elevation model (DEM), and regional geological maps. In this stage, the spectral signature of the five minerals is overlaid on the scatter diagram, resulting in similar absorption at a wavelength of 2 µm, which is interpreted as the absorption of orthophosphate (PO₄). Atmospheric correction was performed on the Landsat 9 images to obtain surface reflectance from the satellite images, then raster extraction of the corrected images was performed focusing only on the 30×30 km studied area. The national digital elevation model (DEMNAS) and Mamuju sheet regional map were used to identify primary phosphate mineralization pathways based on lineament analysis and geological structure interpretation.

The analysis stage combines the data from the preparation stage process including the analysis

of the absorption angle at a wavelength of 2 μ m using the formula for calculating the angle in the triangle concept which produces the gamma angle value (γ). This value will be plotted on the Landsat 9 images using the γ equation formula to see the distribution of pixels that are indicative of phosphate minerals. The pixel density is calculated using the 2×2 km gridding method, and then kriging interpolation is used to determine the distribution pattern. From these steps, the zones indicating phosphate mineral anomalies (PO Zones) were obtained. Conformity analysis with vegetation response and geological control of PO zones was conducted to obtain phosphate mineral anomalies.

The final stage is verification and validation, by ground checking or taking several rock or soil samples in the predetermined anomaly zones. The samples were analyzed at The Intertek Laboratory using X-ray fluorescence (XRF) and Inductively Coupled Plasma-Mass Spectrometry (ICP-MS) methods. The results were validated against the

success ratio of the spectral-wise method. An illustration of the research flow can be seen in the research flowchart (Figure 2).

MATERIALS AND METHODS

Materials

The optical images from Landsat 9 has been used, retrieved from the United States Geological Survey (USGS) satellite data centre (https://earthexplorer.usgs.gov). The Landsat 9 was used to identify anomalies of phosphate minerals based on spectral analysis of the phosphate mineral spectral signature. The atmospheric correction was applied using QGIS version 3.34 Prizren to obtain surface reflectance from satellite images. Detailed satellite images are listed in Tables 1 and 2.

Spectral reflectance data of the apatite minerals were obtained from the USGS Spectral Library at https://crustal.usgs.gov/speclab/ (Table3). The spectral signature of monazite and xenotime has also been used to identify phosphate minerals.

The lineament analysis was carried out to identify the geological structure that controls primary phosphate mineralization. By analyzing struc-

tural patterns, potential areas can be identified for phosphate exploration and better understand the geological processes that lead to mineralization. For the lineament analysis, the national digital elevation model (DEMNAS) 8.3 m resolution was used, obtained from www.tanahair.go.id. Eleven samples have also been measured from the field consisting of rock and soil to verify the proposed method. In addition, nine measured rock samples have also been added from a previous study (Sukadana et al., 2015). Geochemical measurements were carried out at The Intertek Laboratory (www.intertek.com) using X-Ray Fluorescence (XRF) and Inductively Coupled Plasma – Mass Spectrometry (ICP-MS) methods. Phosphate rock content is conventionally expressed as phosphorus pentoxide (P₂O₅), with economic minimum levels of about 5 % (Ptacek, 2016).

Geochemical measurement result shows the P_2O_5 from 0.17 to 1.14 %; K_2O from 0.82 to 12.32 %; and Na_2O from 0.03 to 7.5 %. Reference measured rock samples from the previous study (Sukadana *et al.*, 2015) show the P_2O_5 from 0.17 to 2.73 %; K_2O from 0.54 to 9.88 %; and Na_2O from 1.05 to 6.99 %. The result indicates a good prospect of phosphate-bearing igneous rock.

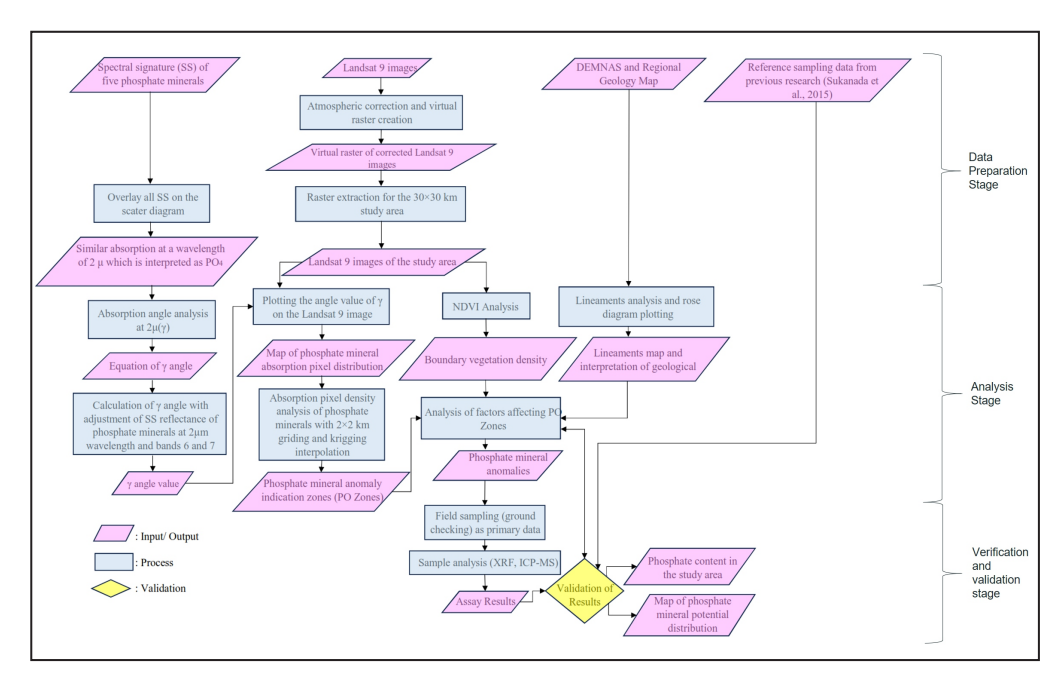


Figure 2. Flowchart of the research to determine the potential distribution of phosphate minerals in the researched location, using Landsat 9 image analysis by applying the equation model (spectral-wise method).

Table 1. Specification of The Data Used in This Study

Image	Criteria	Cloud Cover	Acquired Date	Source	Path/ Frame	Scene ID	Resolution
Landsat-9	Level 1 Collection 2	< 10%	July 27 th , 2023	United States Geological Survey (USGS)	115	LC115062202- 3208LGN00	30×30 m
Digital Elevation Model (DEM)	Single Band Tiff 32 Bit	-	2013	National Digital Elevation Model (DEMNAS)	117	2013-141, 2013-142, 2013-123, 2013-124	8.3×8.3 m
Regional Geology Map	Mamuju Quadrangle, Sulawesi	-	2010	Centre For Geological Survey	2013	Mamuju 2013	1: 250.000

Table 2. An Overview of The Characteristics of The Landsat 9 Images Used in This Study

Day/Month/Year	Band	Name	Centre Wavelength (µm)	Resolution (m)
	B1	Coastal Aerosol	0.443	30
	B2	Visible (blue/B)	0.482	30
	B3	Visible (green/G)	0.562	30
	B4	Visible (red/R)	0.655	30
	B5	Near Infrared (NIR)	0.865	30
27/07/2023	B6	Shortwave Infrared-1 (SWIR-1)	1.610	30
	B7	Shortwave Infrared-2 (SWIR-2)	2.200	30
	B8	Panchromatic	0.590	15
	B9	Cirrus	1.375	30
	B10	Thermal Infrared-1 (TIR-1)	1.080	100
	B11	Thermal Infrared-1 (TIR-1)	1.200	100

Table 3. Specification of The Spectral Signature of Reference Minerals from The USGS Spectral

No	Mineral	Spectral Specification	Sample Origin	Sample Condition
1	Chlorapatite $Ca_{5}(PO_{4})_{3}(Cl)$	splib07a Chlorapatite WS423 ASDFRc AREF	Snarum, Norway	Solid
2	Fluorapatite Ca ₅ (PO ₄) ₃ (F)	splib07a Fluorapatite REE WS418 xtl ASDFRc AREF	Otter Lake, Quebec, Canada	Solid
3	Hydroxylapatite Ca ₅ (PO ₄) ₃ (OH)	splib07a Hydroxyl-Apatite WS425 BECKb AREF	near Cokeville, Wyoming	-
4	Monazite (Ce,La,Th)PO ₄	splib07a Monazite HS255.3B ASDFRb AREF	Miguel County, New Mexico	Powder
5	Xenotime (YPO ₄)	splib07a Xenotime GDS966 Iveland REE ASDFRa AREF	Setesdal, Iveland Municipality, Norway	Solid

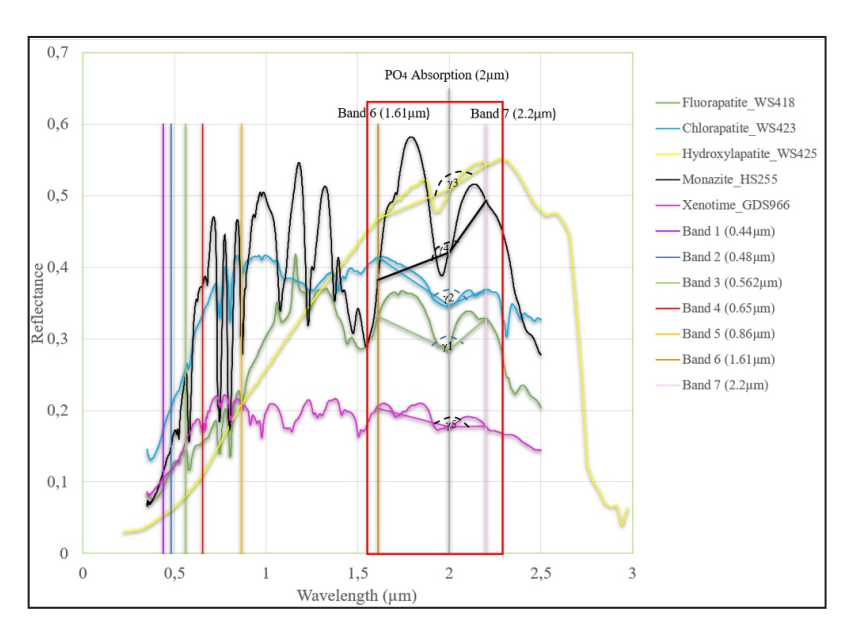
Spectral-Wise Method

The mineral elements have a spectral signature at a certain wavelength as a basis for identification through their spectral signatures (Gupta *et al.*, 2022). The spectral signatures of the five phosphate minerals have been identified in the fluorapatite, chlorapatite, hydroxilapatite, monazite, and xenotime samples (Figure 3). Their spectra show a common absorption pattern at a wavelength of 2 µm due to the absorption of phosphate ion or orthophosphate (PO₄).

The absorption at 2 μ m was located between band 6 and 7 in the Landsat 9 image (Table 2).

Therefore, to identify phosphate minerals in the Landsat 9 image, the absorption angle was carefully been examined between the reflectance at 1.61 μ m (Band 6), 2 μ m (phosphate absorption), and 2.2 μ m (Band 7). The gamma angle γ was then calculated as an intersection of the reflectance line from 1.6 μ m to 2 μ m and 2.2 μ m to 2 μ m, termed as γ 1 to γ 5 (Figure 3).

Calculating the γ , the triangle concept was used as follows (Figure 4). The γ is 180° minus the sum of the tangents α and β , each multiplied by $180^{\circ}/\pi$ to convert from radians to degrees. Tangent α or equal to tangent A/X is the tangent



Spectral reflectance of the five phosphate minerals used in this study (Kokaly et al., 2017), showing similar absorption at a wavelength of 2 µm. The angle among reflectance values at 1.61, 2, and 2.2 µm was used as a basis to identify phosphate minerals.

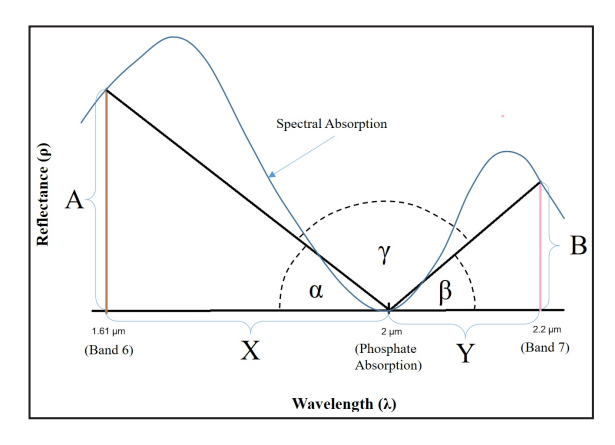


Figure 4. The illustration of the γ in the triangular equation model to estimate phosphate absorption using the Landsat 9 image.

of the spectral absorption curve at Δ reflectance A (between 1.6 and 2 μ m) divided by Δ wavelength X (between 1.6 and 2 μ m), and tangent β or equal to tangent B/Y in the reverse direction (between 2 and 2.2 μ m).

Based on the triangle concept, the γ is expressed as follows:

Where:

A = $\Delta \rho$ between 1.61 μm (band 6) and 2 μm B = $\Delta \rho$ between 2.2 μm (band 7) and 2 μm $X = \Delta \lambda$ between 1.61 μ m (band 6) and 2 μ m $Y = \Delta \lambda$ between 2.2 μ m (band 7) and 2 μ m

To obtain the phosphate index of γ on the Landsat 9 image, the Band 6 and 7, termed as B6 and B7 of Landsat 9, were applied to equation 2 as follows:

$$\lambda = 180^{\circ} - \left(\frac{180^{\circ}}{\pi} \left(\tan \left(\frac{A}{(B7 - 0.2) - B6} \right) + \tan \left(\frac{B}{B7 - (B7 - 0.2)} \right) \right) \right) \dots (2)$$

The dense vegetation covers are a common problem utilizing the remote sensing approach under the Tropics. The dense canopy vegetations serve as an obstacle to the reflected light received by satellite sensors (Prodomou et al., 2022; Wang et al., 2022). To minimize the problem in this study, dense and sparse vegetation were separated using NDVI analysis. The sparse vegetation area was used for mineral assessment. To support the lack of data in areas with dense vegetation, mapping data was used from previous studies. In the same case, if data are available, to minimize this problem leveraging advanced remote sensing techniques were used, such as hyperspectral imaging, LiDAR, and multitemporal data analysis. The accuracy and reliability of lithology identification in vegetated areas can be significantly improved. Furthermore,

exploring potential synergies among different data sources and adopting innovative data fusion methods can contribute to better classification results (Chen et al., 2023). However, the vegetation can respond to the environment in which it grows, such as soil elements, the amount of nutrients, soil moisture, salinity, surface roughness, slope, direction of light, and seasonal changes, including the type of rock (Saepuloh, 2023). The plant responses to soil contamination include tree density, health, height, species distribution, species replacement, growth phase, and aging (Saepuloh, 2023). The stressed vegetation can be assessed by remote sensing as an indicator of radioactivity soil contamination (Saepuloh et al., 2023), hydrothermal alteration (Wu et al., 2024), nutrient deficiency (Mee et al., 2017), or water shortage (Le et al., 2023). Therefore, the normalized difference vegetation index (NDVI) was applied to quickly delineate vegetation and vegetation stress (Huang et al., 2021). The NDVI was used to determine the dense vegetation area (Huang et al., 2021) that might be affecting the reflectance of γ (Chen *et al.*, 2023).

IDENTIFYING PHOSPHATE OCCUR-RENCE BASED ON IMAGE SPECTRAL AND SOIL-VEGETATION RESPONSE Identifying Phosphate Indices

The range of γ from 160.41° has been calculated in fluorapatite to 176.38° in hydroxyapatite samples (Table 6). Following equation (2), the calculated γ of the Landsat 9 image shows an index with an interval from 152° to 200° (Figures 5a, b). For chlorapatite, monazite, and xenotime the interval of γ is from 184° to 208°. The γ is lower than this range, the phosphate mineral threshold is in the 1st quartile (Figures 5c,d,e).

Following the calculation of γ for five selected reference minerals, all y images have been superimposed to identify the occurrences of phosphate minerals based on their pixel density. The density is derived from gridding an area of 2×2 km. The occurrence of γ pixels were counted in each grid and perform kriging interpolation to find out the distribution. To determine the threshold of the phosphate anomaly, the pixel gamma data was plotted on a histogram, resulting in a positive distribution (Figure 6). Based on this distribution, the phosphate anomaly threshold was defined at the 4th quartile or number of pixels greater than 70/ grid (Figure 7a). There are three main phosphate anomaly zones termed as PO Zones, namely Simboro, Mamuju, and Tapalang prospect, named by location of the subdistrict, with a total area of 16,920 Ha (Figure 7b).

Soil-Vegetation Response

The dense vegetation can be a barrier to the reflected light received by satellite sensors (Prodomou *et al.*, 2022; Wang *et al.*, 2022). The Normalized Difference Vegetation Index (NDVI), which standardizes indices to produce images that display greenness (relative biomass), intends to distinguish plants with healthy conditions from plants that are experiencing stress (Saepuloh, 2023). Healthy vegetation can grow better and more densely than stressed vegetation. Thus, the NDVI was used to determine the dense vegetation area that might be affecting the reflectance of γ .

The spectral analysis results show that areas with high γ pixel density are generally directly proportional to high P_2O_5 content, but in some sampling locations, there are opposite results. Based on reference measured rock samples

Table 6. Calculation Results of The γ Based on Equivalent (1) for Phosphate Minerals

Wavelength (λ)	Fluorapatite	Chlorapatite	Hydroxylapatite	Monazite	Xenotime
Band 6 (1.61 µm)	0.331	0.414	0.468	0.382	0.203
PO ₄ (2 μm)	0.285	0.347	0.509	0.421	0.177
Band 7 (2.2 μm)	0.329	0.369	0.543	0.494	0.178
Δ Reflectance (A)	0.046	0.068	-0.042	-0.039	0.026
Δ Reflectance (B)	0.044	0.022	0.034	0.073	0.001
Δ Wavelength (X)	0.390	0.390	0.390	0.390	0.390
Δ Wavelength (Y)	0.200	0.200	0.200	0.200	0.200
Tangent α	6.833	10.027	-6.128	-5.687	3.879
Tangent β	12.753	6.347	9.750	21.784	0.301
Gamma angle (γ)	160.41	163.63	176.38	163.90	175.82

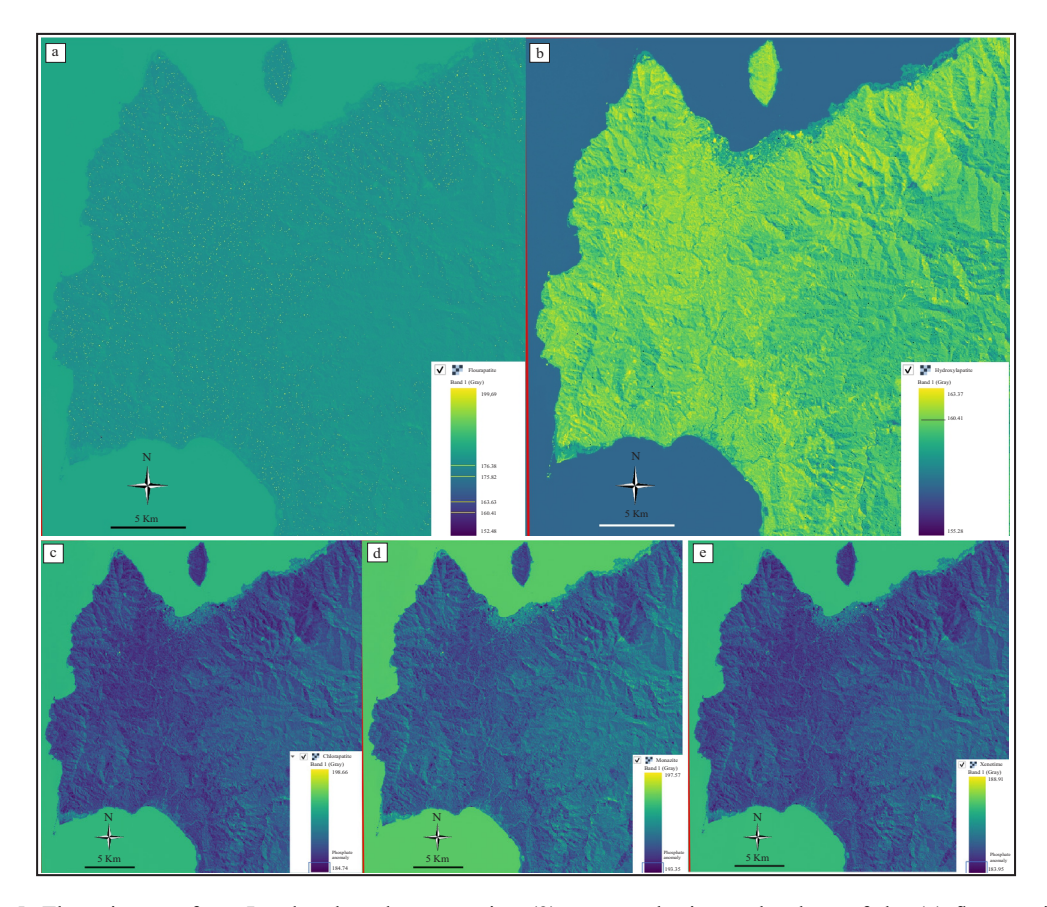


Figure 5. The γ images from Landsat based on equation (2) present the interval values of the (a) fluorapatite; (b) Hydroxylapatite; (c) Chlorapatite; (d) Monazite and (e) Xenotime index minerals. On chlorapatite, monazite, and xenotime minerals, the minimum angle value is at 184.36° (above the maximum gamma angle value), and the phosphate mineral threshold is interpreted to be in quartile 1.

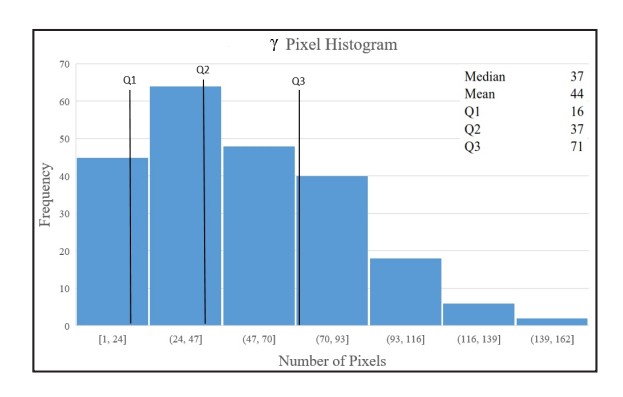


Figure 6. The histogram of γ pixels from Spectral-wise method analysis shows a positive distribution. The anomaly of phosphate is defined in the 4th quartile.

from the previous study (Sukadana *et al.*, 2015), especially in the upstream area of The Mamuju River (Figure 10), it has a high P_2O_5 content of about 2.73 % on MJU118 and 2.67 % on MJU121, but both locations have low γ pixel densities. The overlain with the NDVI image shows that

areas are covered by dense vegetation (Figure 8). that the reflectance in the area was concluded disturbed by the very dense vegetation.

VERIFICATION AND DISCUSSION

Sample analysis results show P₂O₅ values reaching 1.14 % in MMJ603 located in the Ampalas area in The Kalukku Subdistrict (Figure 10). An outcrop on The Ampalas River is a foid syenite rock that is grey to light brown in colour, porphyritic in texture, and hypocrystalline (Draniswari *et al.*, 2020). Phenocrysts are pyroxene, sanidine, leucite, nepheline, alkali feldspar, and plagioclase with aphanitic basement. This outcrop extends for about 30 m on the banks of The Ampalas River, and is generally altered (Figure 9.A),

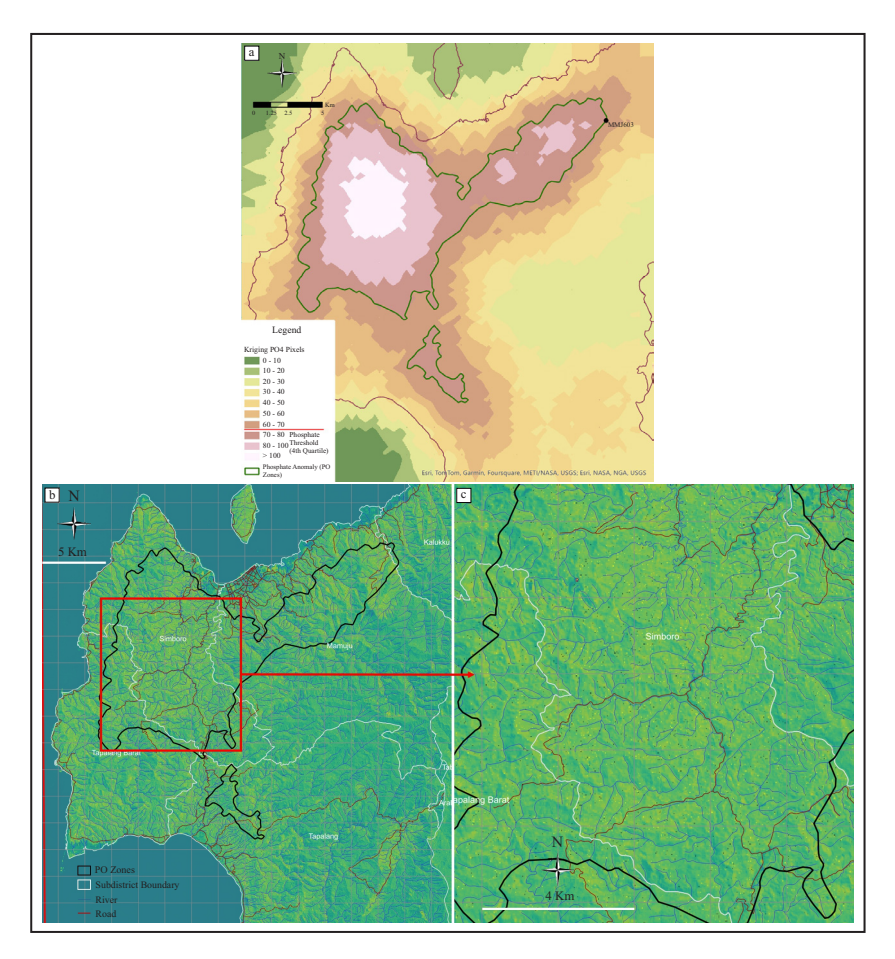


Figure 7. The PO Zones are generated from kriging interpolation of γ pixels from Spectral-wise method analysis. (a)The threshold is defined on the 4th quartile zone. (b) The black point is sampling location for verification in Figure 9; (c) The Superimposed γ image overlain with PO Zones in black polygons, and γ density interpreted as the indicative area of phosphate minerals at Simboro prospect.

indicating the presence of secondary minerals in the form of sulfide minerals such as pyrite and chalcopyrite (Figure 9.B). Referring to the classification of volcanic rocks and based on the content of alkaline minerals and silica plotted on the Total Alkali-Silica (TAS) diagram, it is a tephri-phonolite rock type (Le Bas *et al.*, 1992). In reference to samples from previous research (Sukadana *et al.*, 2015), P₂O₅ reached 2.73 % in MJU118, which is in the upstream area of The Mamuju River in The Mamuju Subdistrict (Figure 10). The plot results on the TAS diagram show the type of phono-tephrite rock.

Both tephri-phonolite and phono-tephrite are volcanic rocks with high potassium content, with total alkali of up to 12.53 %. PO Zones are mostly found in the western to northern part of the studied area, which is the Simboro and

Mamuju prospect, and some appear in the middle part, which is the Tapalang prospect. Following the concentration of potassium minerals in West Sulawesi (Sukadana *et al.*, 2021), about 15 % of PO Zones are in the high potassium zones (Figure 10). This part is interpreted as the main concentration of phosphate minerals.

Analysis of the lineaments which is carried out by interpreting the straightness in the morphology of ridges and valleys which aims to determine its relation with the developing geological structure as well as its relation with indications of certain mineralization processes (Indrastomo *et al.*, 2017). This analysis shows that the main lineaments is southwest - northeast, in line with the main structural pattern in the regional geology (Ratman and Atmawinata, 2010) and the PO Zone distributions (Figure 11).

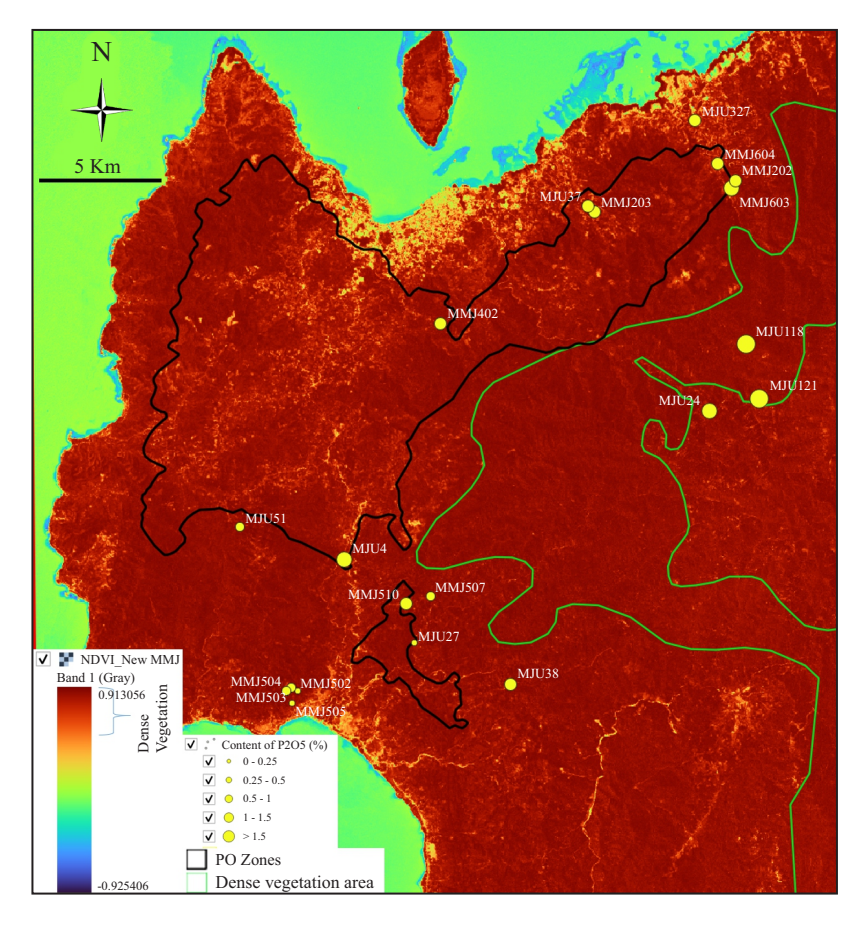


Figure 8. The NDVI image shows the dense vegetation presented by dark red. The light green polygonal line is the boundary.



Figure 9. Outcrop of (a) altered foid syenite at the northern part of the studied area for sampling location MMJ603; (b) The presence of secondary minerals in the form of sulfide minerals such as pyrite and chalcopyrite, in dark grey sections; and (c) hand specimen of altered foid syenite in The Ampalas River, Kalukku Subdistrict, West Sulawesi. The sampling locations are depicted in Figure 7a.

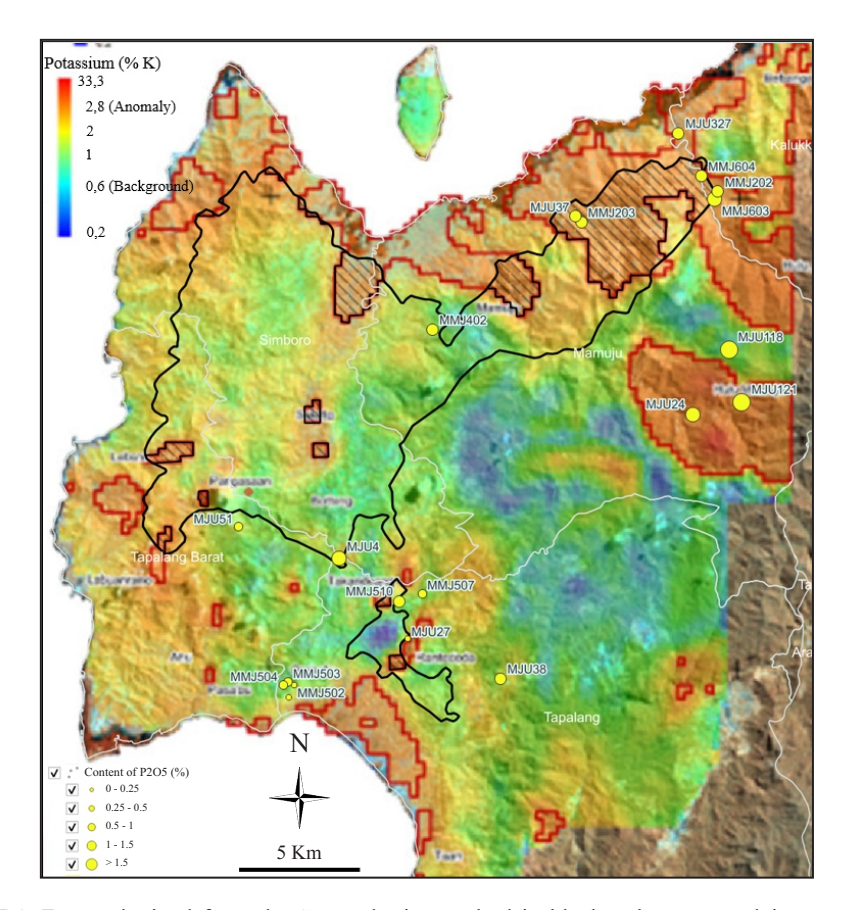


Figure 10. The PO Zones obtained from the Spectral-wise method in black polygons overlain on the potassium (K) concentration map (modification from Sukadana *et al.*, 2021). Red polygons show areas of high potassium, and the black-shaded polygons are intersecting areas with PO Zones.

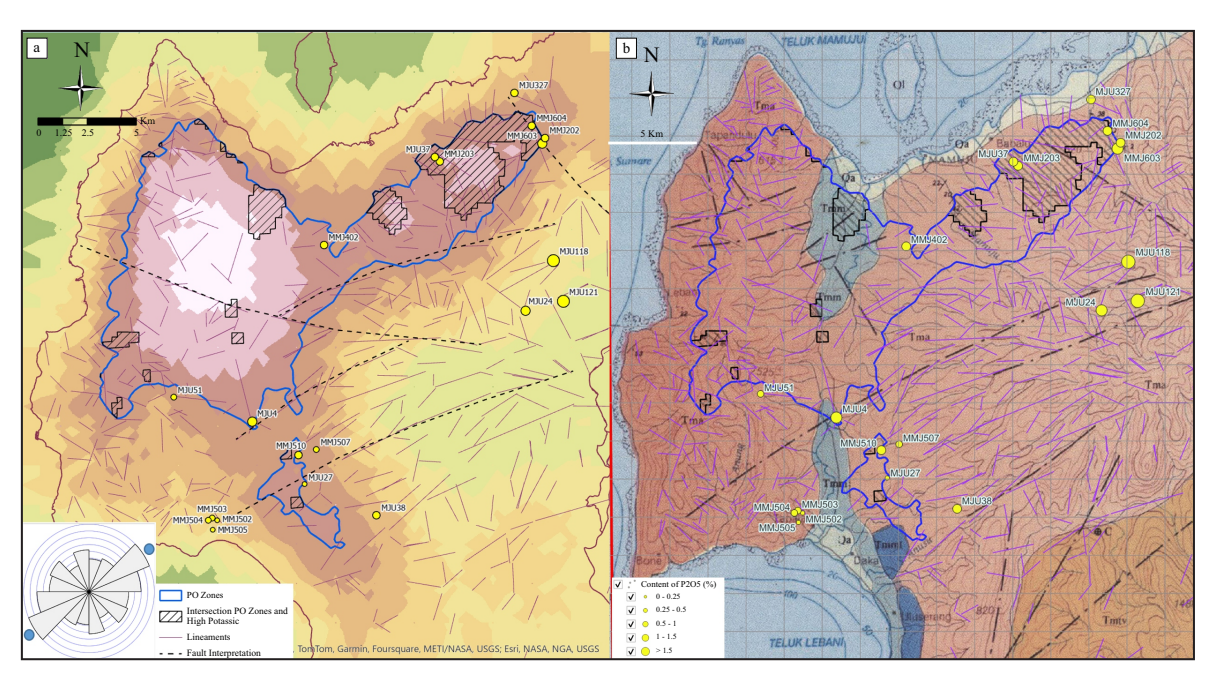


Figure 11. The identified geological lineaments developed in the studied area based on visual observation using the shaded map of The National Digital Elevation Model (DEMNAS) produce the rose diagram showing the main direction of the southwest –northeast (a). Overlaid with the regional geological map of Mamuju (Ratman and Atmawinata, 2010), the lineaments show in accordance with the direction of the main fault (b).

Conclusion

The spectral absorption of fluorapatite, chlorapatite, hydroxylapatite, monazite, and xenotime minerals at a wavelength of 2 μm is the absorption of orthophosphate (PO₄). The Spectralwise method has been applied successfully to determine the orthophosphate in the Landsat 9 image. The phosphate mineral indication area (PO Zones) was determined by the pixel density of the orthophosphate absorption. The Spectral-wise method detected three prospect areas at Simboro, Mamuju, and Tapalang about 16,920 Ha. Based on the concentration of potassium minerals in West Sulawesi, about 2,604 Ha or 15 % of the PO Zone is located in the high potassium zone.

Ground check sampling verified that the eight samples were located precisely at The PO Zones and the twelve samples around the PO Zones. Those samples had a higher P₂O₅ concentration than those outside The PO Zones. The three samples in the upstream area of The Mamuju River were excluded due to dense vegetation covers presented by the normalized difference vegetation index (NDVI) with a pixel value index of more than 0.7. Based on the P₂O₅ sampling location, the correctness of the Spectral-wise method have been calculated, that is about 70 %. The problem was primarily due to vegetation cover, the dense canopy vegetation served as an obstacle affecting the reflectance of γ . To find the representative data, dense and sparse vegetation were separated and used only the sparse vegetation area for mineral assessment. Sapping data was used from previous studies to support the lack of data in areas with dense vegetation. In the same case, to minimize this problem one can also explore potential synergies among different data sources and adopt innovative data fusion methods.

Based on the lineament analysis, The PO Zones at the western part were in concordance with the SW–NE strike-slip fault on the regional geology of Mamuju. The PO Zones at the southwest to northeast are also in concordance with those strike slip fault. Therefore, The PO Zones in the studied area occurs at an intensive geological structures in SW–NE direction.

ACKNOWLEDGEMENT

The author would like to express sincere gratitude to Mr. Robby Rafianto, Head of the Exploration and Mine Development Department at PT Trimegah Bangun Persada Tbk., for his invaluable support and insightful advice throughout this research. Appreciation is also extended to Mr. Tri Hadi Nugraha and Mr. Gunawan Dwijatmiko for their assistance in collecting field data. Additionally, the use of Landsat-9 satellite imagery, courtesy of the U.S. Geological Survey, greatly contributed to the success of this study.

REFERENCE

Abdullah, S., Ertürk, M.A., and Yalçin, C., 2023. *Alkaline Igneous Rocks*, Bidge Publications.

Chen, Y., Wang, Y., Zhang, F., Dong, Y., Song, Z., and Liu, G., 2023. Remote Sensing for Lithology Mapping in Vegetation-Covered Regions: Methods, Challenges, and Opportunities, *Minerals*, 13 (9). DOI: 10.3390/min13091153.

Ciputra, R.C., Pratiwi, F., Putra, A.F., Syaeful, H., Indrastomo, F.D., Adimedha, T.B., and Sukadana, I.G.,2025. Makassar Strait Thrust - Mamuju Segment (MSTM) Perspective on Radioactive Mineral Exploration: A Case Study in Rantedoda, Mamuju. *Indonesian Journal on Geoscience*, 12 (3), p.319-34. DOI: 10.17014/ijog.12.3.319-341

Draniswari, W., Kusuma, S., Adimedha, T., and Sukadana, I., 2020. Peran Kontaminasi Kerak pada Diferensiasi Magma Pembentuk Batuan Vulkanik Sungai Ampalas, Mamuju, Sulawesi Barat. *EKSPLORIUM*, 41 (2). DOI: 10.55981/eksplorium.2020.6040.

Gupta, D.K., Prashar, S., Singh, S., Srivastava, P.K., and Prasad, R., 2022. Chapter 1 - Introduction to RADAR remote sensing, p.3-27. *In*: Srivastava, P.K., Gupta, D.K., Islam, T., Han, D., and Prasad, R. (eds.). *Radar Remote Sensing*, Elsevier. DOI: 10.1016/B978-0-12-823457-0.00018-5.

Huang, S., Tang, L., Hupy, J.P., Wang, Y., and Shao, G., 2021. A commentary review on the

- use of normalized difference vegetation index (NDVI) in the era of popular remote sensing. *Journal of Forestry Research*, 32 (1), p.1-6. DOI: 10.1007/s11676-020-01155-1.
- Indrastomo, F. D., Sukadana, I., Saepuloh, A., and Handoyo, A., 2015. Integrated Radiometric Mapping using Field-Based and Remote Sensing Techniques for Uranium and Thorium Exploration at Mamuju Region, West Sulawesi, Indonesia, *Proceedings Joint Convention Balikpapan*, 2015.
- Indrastomo, F. D., Sukadana, I. G., and Suharji, S., 2017. Identifikasi Pola Struktur Geologi Sebagai Pengontrol Sebaran Mineral Radioaktif Berdasarkan Kelurusan Pada Citra Landsat-8 di Mamuju, Sulawesi Barat, *Eksplorium*, 38 (2), p.71-80. DOI: 10.55981/ eksplorium.2017.3874
- Khairani, M., Sutrisno, and Indrastomo, F.D., 2018. *Identifikasi Uranium Dan Thorium Di Desa Takandeang, Mamuju Sulawesi Barat Dengan Menginterpretasikan Data Radiometri Tanah Atau Batuan*, Fakultas Sains Dan Teknologi Universitas Islam Negeri Syarif Hidayatullah Jakarta, 1 (1), p.1-8.
- Kokaly, R.F., Clark, R.N., Swayze, G.A., Livo,
 K.E., Hoefen, T.M., Pearson, N.C., Wise,
 R.A., Benzel, W., Lowers, H.A., Driscoll,
 R.L., and Klein, A.J., 2017, USGS Spectral Library Version 7 (Report 1035), Reston, VA,
 retrieved from USGS Publications Warehouse,
 68. DOI: 10.3133/ds1035.
- Le Bas, M.J., Le Maitre, R.W., and Woolley, A.R., 1992, The construction of the Total Alkali-Silica chemical classification of volcanic rocks. *Mineralogy and Petrology*, 46 (1), p.1-22. DOI: 10.1007/BF01160698.
- Le, T.S., Harper, R., and Dell, B., 2023. Application of Remote Sensing in Detecting and Monitoring Water Stress in Forests. *Remote Sensing*, 15 (13). DOI: 10.3390/rs15133360.
- Mee, C.Y., Balasundram, S.K., and Hanif, A.H.M., 2017. Detecting and Monitoring Plant Nutrient Stress Using Remote Sensing Approaches: A Review. *Asian Journal of Plant Sciences*, 16, p.1-8.

- Prodromou, M., Gitas, I., Themistocleous, K., and Hadjimitsis, D., 2022. The implementation of the Forest Canopy Density (FCD) model for Coniferous ecosystems in Cyprus forests, using Landsat-8 and Sentinel-2 satellite data., *Presented at the EGU General Assembly Conference Abstracts*, EGU22-9865.
- Ptáček, P., 2016. Phosphate Rocks, Ch. 7. *In*: Petr Ptacek (ed.). *Apatites and their Synthetic Analogues*, IntechOpen, Rijeka. DOI: 10.5772/62214.
- Ratman, N. and Atmawinata, S., 2010. *Geological map of Mamuju Quadrangle, Sulawesi 1:250.000*, Geological Research and Development Centre of Indonesia.
- Saepuloh, A., Ratnanta, I.R., Hede, A.N.H., Susanto, V., and Sucipta, I.G.B.E., 2023. Radioactive remote signatures derived from Sentinel-2 images and field verification in West Sulawesi, Indonesia. *Environmental Monitoring and Assessment*, 195 (10), 1243p. DOI: 10.1007/s10661-023-11868-5.
- Saepuloh, A., 2023. *Prinsip Geobotanical Remote Sensing*, Presented at the Remote Sensing Geology Courses, FITB ITB, Bandung.
- Shaban, G., Fadlin, and Priadi, B., 2016. Geochemical Signatures of Potassic to Sodic Adang Volcanics, Western Sulawesi: Implications for Their Tectonic Setting and Origin. *Indonesian Journal on Geoscience*, 3 (3), p.195-214. DOI: 10.17014/ijog.3.3.195-214.
- Steiner, G., Geissler, B., Watson, I., and Mew, M.C., 2015. Efficiency developments in phosphate rock mining over the last three decades. *Losses and Efficiencies in Phosphorus Management*, 105, p.235-245. DOI: 10.1016/j. resconrec.2015.10.004.
- Sukadana, I.G., Harijoko, A., and Setijadji, L.D., 2015. Tataan Tektonika Batuan Gunung Api di Kompleks Adang Kabupaten Mamuju Provinsi Sulawesi Barat. *Eksplorium*, 36 (1), p.31-44.
- Sukadana, I.G., Warmada, I Wayan, Harijoko,A., Indrastomo, F.D., and Syaeful, H., 2021.The Application of Geostatistical Analysis on Radiometric Mapping Data to Recognized the Uranium and Thorium Anomaly

- in West Sulawesi, Indonesia. *IOP Conference Series: Earth and Environmental Science*, 819 (1), 012030. DOI: 10.1088/1755-1315/819/1/012030.
- Wang, H., Muller, J.D., Tatarinov, F., Yakir, D., and Rotenberg, E., 2022. Disentangling Soil, Shade, and Tree Canopy Contributions to Mixed Satellite Vegetation Indices in a Sparse Dry Forest. *Remote Sensing*, 14 (15). DOI: 10.3390/rs14153681.
- Wu, Y., Shao, C., Zhang, J., Liu, Y., Li, H., Ma, L., Li, M., Shen, B., Hou, L., Chen, S., Xu,
- D., Xin, X., and Liu, X., 2024. Elevation-Dependent Contribution of the Response and Sensitivity of Vegetation Greenness to Hydrothermal Conditions on the Grasslands of Tibet Plateau from 2000 to 2021. *Remote Sensing*, 16 (1). DOI: 10.3390/rs16010201.
- Xu, C., Dai, Q., Gaines, L., Hu, M., Tukker, A., and Steubing, B., 2020. Future material demand for automotive lithium-based batteries. *Communications Materials*, 1 (1), 99pp. DOI: 10.1038/s43246-020-00095-x.